

# C I 492 GHz mapping toward Cas A

B. Mookerjea<sup>1,2\*</sup>, N. G. Kantharia<sup>3†</sup> D. Anish Roshi<sup>4‡</sup>, M. Masur<sup>2§</sup>

<sup>1</sup>*Department of Astronomy, University of Maryland, College Park, MD 20742, USA*

<sup>2</sup>*KOSMA, I. Physikalisches Institut, Universität zu Köln, Zùlpicher Strasse 77, 50937 Köln, Germany*

<sup>3</sup>*National Centre for Radio Astrophysics, TIFR, Post Bag 3, Ganeshkhind, Pune 411007, India*

<sup>4</sup>*Raman Research Institute, Sadashivanagar, Bangalore 560 080, India*

Accepted . Received ; in original form

## ABSTRACT

We have mapped the [C I]  $^3P_1-^3P_0$  emission at 492 GHz toward the supernova remnant Cas A. We detect [C I] emission from the periphery of the diffuse Photon Dominated Region (PDR) covering the disk of Cas A, as traced by the carbon recombination lines, as well as from the denser PDRs associated with the molecular clouds towards the south-east. [C I] emission is detected from both the Perseus and Orion arm molecular clouds, with the  $-47 \text{ km s}^{-1}$  Perseus arm feature being strong enough to be detected at all positions. We estimate the C/CO relative abundance to be 0.2 at the position of the identified CO clouds and  $> 1$  for most of the cloud. Here we show that the distribution of [C I] emitting regions compared to the  $C^+$  region and molecular cloud is consistent with a scenario involving PDRs. Using physical models for PDRs we constrain the physical properties of the [C I] line-forming regions. We estimate the densities of the [C I] emitting regions to be between  $10^2$  and  $10^3 \text{ cm}^{-3}$ . Based on rather high volume filling factors ( $\sim 50\%$ ) we conclude that [C I] emission mainly arises from diffuse neutral gas in the Perseus arm.

**Key words:** ISM:general – ISM:lines and bands – ISM:molecules – ISM:clouds – radio lines:ISM – radio lines:general – Galaxy:general.

## 1 INTRODUCTION

Molecular clouds are embedded in the diffuse interstellar medium (ISM) of the Galaxy where most of the gas is in an atomic form. The atomic gas is mostly located in two phases that are in pressure equilibrium, the cold neutral medium (CNM) with temperatures of  $T \sim 100 \text{ K}$  and the warm neutral medium (WNM) with  $T \sim 10^4 \text{ K}$  (Kulkarni & Heiles 1987; Dickey & Lockman 1990; Wolfire et al. 2003; McKee et al. 2004). Some of the cold atomic gas is also associated with the denser molecular clouds, possibly forming an extended halo or envelope (Andersson & Wannier 1993; Moriarty-Schieven et al. 1997).

Far-ultraviolet (FUV) photons ( $6.0 < h\nu < 13.6 \text{ eV}$ ) from OB stars produce Photon Dominated Regions (PDRs) either at the interface between the H II region and the molecular cloud (classical high density PDRs) or in neutral components (atomic or molecular) of the diffuse interstellar

medium (diffuse PDRs). PDRs are defined as neutral regions where the chemistry and heating are regulated by the FUV photons (Hollenbach et al. 1999). Current understanding of PDRs suggest chemical stratification in which with increasing depth from the surface of the PDR, the dominant carbon-bearing species changes from  $C^+$  through  $C^0$  to CO. Observations of [C II], [C I] and CO lines tracing the different layers of PDRs is thus a useful tool to constrain various conditions of the PDRs.

Ionized carbon in dense star forming regions is mainly traced using the  $^2P_{3/2}-^2P_{1/2}$  fine structure line at  $158 \mu\text{m}$  (Howe et al. 1991; Mookerjea et al. 2003). The radio observations of carbon recombination lines (RRLs) provide a very good alternative way to trace the spatial distribution of ionized carbon. Classical C II regions which form part of high-excitation PDRs, are usually identified through the observation of narrow ( $4 - 10 \text{ km s}^{-1}$ ) carbon RRLs at frequencies  $> 1 \text{ GHz}$  toward H II regions (Pankonin et al. 1977; Wyrowski et al. 2000) and have been well studied. The diffuse C II regions which form part of low-excitation PDRs, are identified through observations of carbon RRLs in absorption at frequencies below  $\sim 150 \text{ MHz}$  and in emission above  $\sim 200 \text{ MHz}$  (Payne et al. 1989).

\* E-mail: bhaswati@astro.umd.astro.edu

† E-mail: ngk@ncra.tifr.res.in

‡ E-mail: anish@rri.res.in

§ E-mail: masur@ph1.uni-koeln.de

Diffuse C II regions were discovered more than two decades ago through the detection of carbon RRL in absorption at 26.3 MHz (C631 $\alpha$ ) in the direction of Cas A (Konovalenko et al. 1980; Blake et al. 1980). Since then several RRLs spanning over 14 to 1400 MHz have been observed in this direction (Kantharia et al. 1998, and references therein) and it remains the only diffuse C II region which has been studied and modelled in such detail using C RRL. A smooth transition of lines in absorption at frequencies below 115 MHz to lines in emission at frequencies above 200 MHz has been detected (Payne et al. 1989, see Fig. 1). Moreover, this is the only direction in the Galaxy where high resolution ( $\sim 1'$ ) image of the diffuse C II region in carbon RRLs near 332 MHz exist (Kantharia et al. 1998, see Fig 2). Modeling the line emission in this direction shows that the carbon RRLs originate in cold regions with  $T_e = 75$  K and  $n_e = 0.02$  cm $^{-3}$  (Kantharia et al. 1998). Several molecular line studies have been performed towards the direction of Cas A. These observations do not detect much CO emission from the disk of Cas A, but identify molecular clumps located primarily to the south east of the disk (Troland et al. 1985; Wilson et al. 1993; Liszt & Lucas 1999). The diffuse C II regions could be coexistent with the cold neutral medium (CNM) that produce H I absorption toward Cas A (Payne et al. 1994) or with the molecular component of the interstellar medium (ISM) (Ershov et al. 1987). In the direction of Cas A, a morphological comparison of C RRL distribution with that of H I and  $^{12}\text{CO}$  indicate that the C RRL emission is more likely associated with H I gas (Kantharia et al. 1998).

The upper state of the [C I]  $^3\text{P}_1\text{-}^3\text{P}_0$  transition at 492 GHz is only 23 K above ground. For this transition, the critical density for collisions with  $\text{H}_2$  molecules is only 1000 cm $^{-3}$  (Schröder et al. 1991). This implies that [C I] is easily excited and also the line is easily detectable even when emitted by moderate density interstellar gas exposed only to a radiation field equal to the mean interstellar radiation field in the solar neighborhood. Thus [C I] can be used as a reliable tracer of the diffuse PDRs as well. Here we present [C I] mapping observations at 492 GHz in the direction of Cas A in order to probe whether the [C I] emission like the C RRL emission arise solely from the atomic CNM or the molecular phase also contributes to it. We have compared the [C I] observations with the C270 $\alpha$ , H I,  $^{12}\text{CO}$  2-1 and  $^{13}\text{CO}$  1-0 observations available in literature and have used PDR models to explain the neutral carbon and CO emission wherever the two spatially overlap.

## 2 OBSERVATIONS AND DATA ANALYSIS

We have mapped the Cas A region in the fine structure transition  $^3\text{P}_1\text{-}^3\text{P}_0$  at 492 GHz of atomic carbon using the Submillimeter Array Receiver for Two frequencies (SMART; Graf et al. 2002) on KOSMA (Winnewisser et al. 1986), a 3-m submillimeter telescope located on the Gornergrat in Switzerland. SMART is a dual-frequency eight-pixel SIS-heterodyne receiver that observes simultaneously at 4 positions (separated by 116'') on the sky at two frequencies in the range 455-495 GHz and 795-882 GHz. The IF signals are analyzed with array-acousto-optical spectrometers (array-AOSs). The array-AOS consists of 4 AOSs each with

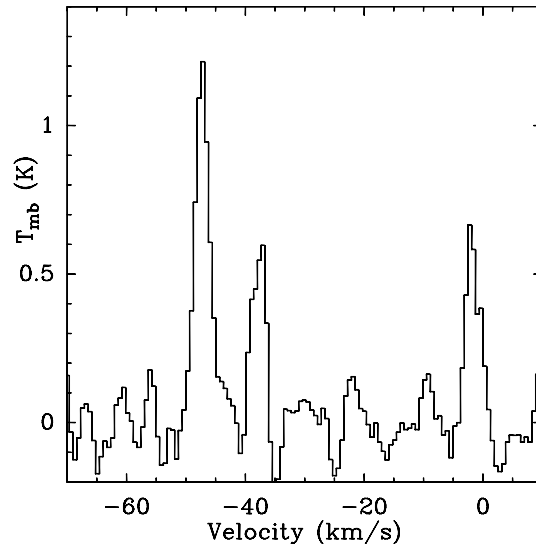


**Figure 1.** [C I] spectrum towards Cas A averaged over part of the observed region, limited in the west to  $\Delta\alpha = -80''$  and in the north to  $\Delta\delta = 80''$ . The Perseus arm and Orion arm components are clearly detectable. The effective velocity resolution of the spectrum is  $0.63$  km s $^{-1}$ .

a bandwidth of 1 GHz and a spectral resolution of 1.5 MHz (Horn et al. 1999). This corresponds to a velocity resolution of  $0.63$  km s $^{-1}$  at the frequency of the [C I] line. Owing to technical difficulties the higher frequency channel of SMART could not be used during our observations. Typical receiver noise temperature achieved at the center of the bandpass at 492 GHz is 150 K. Based on cross-scans on Jupiter at 492 GHz we estimated the HPBW to be  $55''$  and the beam efficiency ( $\eta_{\text{mb}}$ ) to be 50%.

We observed a fully sampled map centred at Cas A ( $\alpha_{2000} = 23^{\text{h}}23^{\text{m}}24^{\text{s}}$ ;  $\delta_{2000} = +58^{\circ}48'.9$ ), extending over  $\sim 6' \times 7'$ . The observations were done in the On-The-Fly (OTF) position switched mode, with the reference position being  $2^{\circ}$  south of the map centre. The map presented in this paper required 5 complete coverages of the region and the total integration time per position on the sky was 50 seconds. The atmospheric calibration were done by measuring the atmospheric emission at the reference position to derive the opacity (Hiyama 1998) and the sideband imbalances were corrected for using standard atmospheric models (Cernicharo 1985).

Data was analyzed using the GILDAS<sup>1</sup> spectroscopic data reduction package. Sinusoidal baselines were subtracted in order to correct for the standing waves.

## 3 RESULTS

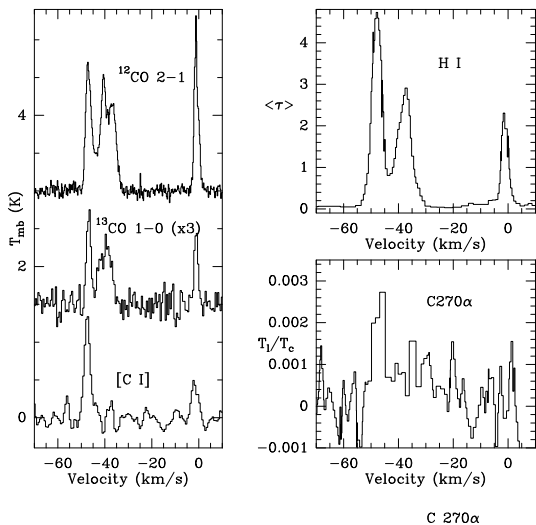
### 3.1 Velocity Structure in [C I]

Figure 1 shows the observed [C I] spectrum averaged over part of the map restricted in the west to  $\Delta\alpha = -80''$  and in the north to  $\Delta\delta = 80''$ . We identify mainly three strong emission features, at  $-47$  km s $^{-1}$  and  $-38$  km s $^{-1}$  corresponding to the Perseus arm and at

<sup>1</sup> <http://www.iram.fr/IRAMFR/GILDAS>

**Table 1.** Results of Gaussian fits to the average spectral profiles of [C I],  $^{12}\text{CO}$  2–1,  $^{13}\text{CO}$  1–0, C270 $\alpha$  and optical depth spectrum of H I.

Line	Component	Centroid km s $^{-1}$	Width km s $^{-1}$
[C I]	Perseus arm	$-47.4 \pm 0.1$	$2.9 \pm 0.2$
	Orion arm	$-1.7 \pm 0.1$	$3.1 \pm 0.4$
$^{12}\text{CO}$ 2–1		$-46.9 \pm 0.01$	$3.0 \pm 0.05$
	Perseus arm	$-40.3 \pm 0.01$	$4.5 \pm 0.07$
	Orion arm	$-36.2 \pm 0.03$	$3.0 \pm 0.07$
$^{13}\text{CO}$ 1–0	Perseus arm	$-46.8 \pm 0.05$	$2.1 \pm 0.1$
		$-39.7 \pm 0.15$	$6.1 \pm 0.3$
	Orion arm	$-1.1 \pm 0.06$	$1.8 \pm 0.14$
C270 $\alpha$	Perseus arm	$-46.8 \pm 0.6$	$5.1 \pm 0.9$



**Figure 2.** Left panel: Average spectra of [C I],  $^{12}\text{CO}$  2–1,  $^{13}\text{CO}$  1–0 emission. Right panel: *Bottom*: Average spectrum of C270 $\alpha$  in units of line to continuum ratio and *Top*: Average spectrum of H I optical depth. All spectra are averaged over the disk of Cas A.

$-1 \text{ km s}^{-1}$  corresponding to the local Orion arm. Since the  $-38 \text{ km s}^{-1}$  feature and the Orion arm feature do not appear at all positions within the mapped region, the spectrum obtained by averaging over the entire mapped region does not show them clearly. Thus, in order to provide a fair representation of all velocity components detected in the region we show here the average spectrum over the selected region.

Figure 2 shows a comparison of the emission spectra of [C I],  $^{13}\text{CO}$  1–0,  $^{12}\text{CO}$  2–1, C270 $\alpha$  (at 332 MHz) and the optical depth spectrum of H I, all averaged over the disk of Cas A. The CO spectra are from the observations by Liszt & Lucas (1999), the C270 $\alpha$  spectrum was observed by Kantharia et al. (1998), and the H I optical depth spectrum is from Schwarz et al. (1997). Table 1 presents the results of fitting Gaussian components to the average emission spectra of the different tracers. The  $-47 \text{ km s}^{-1}$  Perseus arm and the  $-1 \text{ km s}^{-1}$  Orion arm features (not in C270 $\alpha$ ) are detected most clearly in all the emission and absorption spectra. The

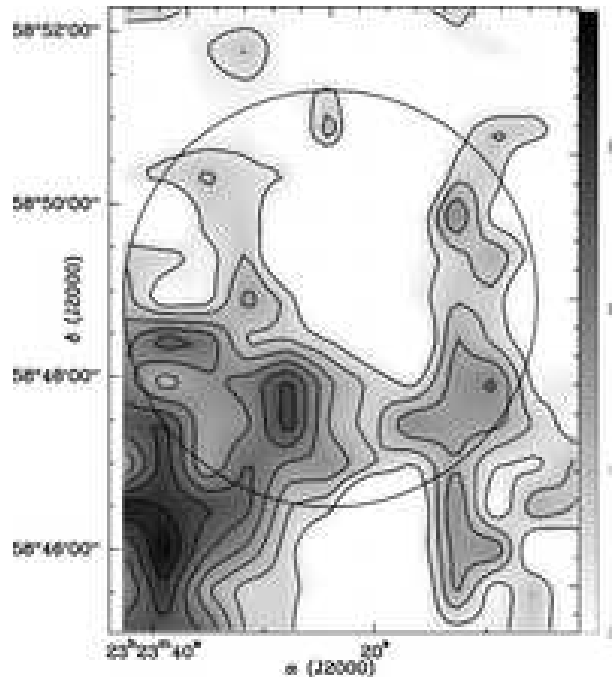


**Figure 3.** Distribution of [C I] emission from Cas A. The intensities are integrated between  $-50.3$  and  $-44.1 \text{ km s}^{-1}$ . Contours range 28 to 98% (in steps of 10%) of the peak ( $9.7 \text{ K km s}^{-1}$ ). Circle denotes the extent of the Cas A disk.

$^{12}\text{CO}$  2–1 emission shows two more Perseus arm features nominally around  $-39$  and  $-36 \text{ km s}^{-1}$ . The [C I],  $^{13}\text{CO}$  and H I data do not resolve the two Perseus arm features at  $-39$  and  $-36 \text{ km s}^{-1}$ , rather show a single feature at  $\sim -38 \text{ km s}^{-1}$ . Although the C270 $\alpha$  spectrum shows mainly the  $-47 \text{ km s}^{-1}$  feature, the same gas as traced by C RRLs with different  $\alpha$ s also shows the  $-38 \text{ km s}^{-1}$  feature both in emission and absorption (*cf.* Fig. 1, Payne et al. 1989).

All tracers appear to show rather similar velocity components. Thus based on velocity features it is not possible to isolate the contribution of atomic and molecular components of the neutral ISM towards the observed [C I] emission.

Rest of the paper discusses the  $-47 \text{ km s}^{-1}$  Perseus arm feature which is detected in all tracers.

### 3.2 [C I] emission from the Perseus Arm at $-47 \text{ km s}^{-1}$

Figure 3 shows the intensity map of [C I] emission from the Perseus arm clouds along the line of sight to Cas A (the circle denotes the extent of Cas A), integrated between the velocities of  $-50.3$  and  $-44.1 \text{ km s}^{-1}$ . The observed [C I] emission toward Cas A consists of two distinct morphological features. The first feature is the bright emission detected towards the south-east and the second is the filamentary structure to the west of the map extending almost north-south. There is almost no emission detected from the northern part of the disk of Cas A.

Figure 4 shows the channel maps of [C I] emission between velocities  $-49.7 \text{ km s}^{-1}$  to  $-44.7 \text{ km s}^{-1}$ . It shows that the emission from the cloud to the south-east covers the largest range of velocities between  $-48.5$  to  $-45.9 \text{ km s}^{-1}$ .

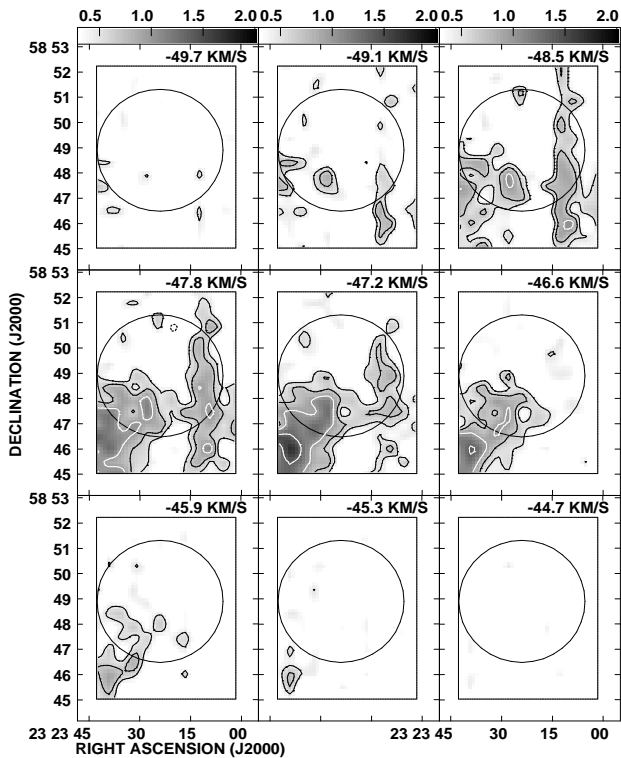


**Figure 4.** Channel maps of CI emission. The circle denotes the extent of Cas A. Velocity is labelled in each panel. The grey scale ranges from 0.32 to 2 K and contours are plotted for 0.48, 0.68, 0.96 and 1.35 K. Note the wider south-east component of [C I].

The linear filamentary extension in the west in contrast is detected only between  $-49.1$  to  $-47.2$   $\text{km s}^{-1}$ .

The morphology of [C I] emission rules out interaction of this gas with the SNR. As shown in Fig. 4, the [C I] emission is seen mostly from the southern part of the supernova remnant; the eastern part coincides with the molecular cloud seen in that region (Wilson et al. 1993) which is also believed to lie in the Perseus arm but not interacting with Cas A. If there was interaction between [C I] line emitting region and Cas A then it would lead to one of the following being true: a) if the line emission is affected by the continuum from Cas A then it should show good morphological correlation with the supernova remnant (SNR). However this is not the case here. b) peculiar spectral features from the regions close to Cas A e.g. broad lines or stronger lines. No such trend is seen and this also helps rule out any interaction between the two. Thus, we believe that the [C I] gas is not interacting with the supernova remnant.

### 3.3 Comparison of [C I], C270 $\alpha$ & H I distribution: Atomic Gas

Figure 5 shows the [C I] emission superposed on the contours of C270 $\alpha$  optical depth (Kantharia et al. 1998) both at velocities of  $-48$   $\text{km s}^{-1}$ . While the [C I] emission overlaps partially with the C270 $\alpha$  emission, it also appears to surround

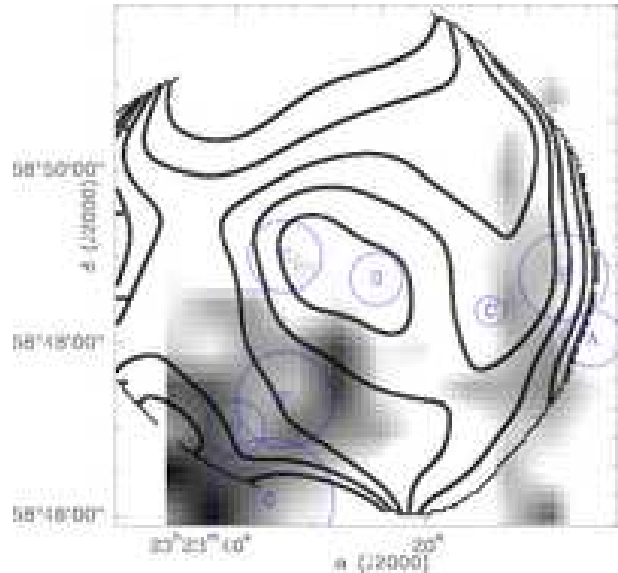


**Figure 5.** Comparison of [C I] (gray scale) channel (of  $1.4$   $\text{km s}^{-1}$  width) map with C270 $\alpha$  optical depth (black contours) (Kantharia et al. 1998) centred at a velocity of  $-48.0$   $\text{km s}^{-1}$ . The circles show the CO clouds identified by Wilson et al. (1993). The contour levels are 1, 2, 3, 4, 5, 7, 9 and 11 in units of 0.001. The greyscale ranges between 2 and  $9.8$   $\text{K km s}^{-1}$ .

the C270 $\alpha$  emitting region and there are some significant differences in morphology between the two. The C270 $\alpha$  peak optical depth is observed from the central part of Cas A and is not coincident with the [C I] peak. The [C I] peak is located to the south of the C270 $\alpha$  peak which possibly indicates the chemical stratification from  $\text{C}^+$  through  $\text{C}^0$  to CO.

The location of the peak of the C RRL emission at the centre of the SNR in Cas A is indeed intriguing. Assuming that the observed line width of recombination lines at 34.5 MHz was entirely due to radiation broadening, Kantharia et al. (1998) put a lower limit on the distance of 115 pc between the line forming region and Cas A indirectly ruling out the association of this gas with the SNR. On the other hand, Kassim et al. (1995) have reported flatter spectrum in the central arcmin or so of Cas A at frequencies below 330 MHz. The common location of the recombination line gas and the absorbing gas is intriguing and argues for a common origin. However, Kassim et al. (1995) argue that the thermal absorbing gas is located within Cas A in which case a common origin of the gas is ruled out. Moreover the carbon recombination line forming gas has a continuum optical depth of  $6.4 \times 10^{-4}$  at 74 MHz which is much less than the optical depth (1.3) of the gas that Kassim et al. (1995) detect. We conclude that the positional coincidence of the carbon recombination line forming gas and the flat spectrum region towards Cas A does look fairly intriguing and demands further investigation.

The line of sight to Cas A has provided a uniquely detailed set of observations of RRLs from highly excited states of singly ionized carbon (e.g. Konovalenko et al. 1980; Ershov et al. 1987; Payne et al. 1989; Anantharamaiah et al. 1994; Kantharia et al. 1998). Interpretation of these RRLs using models considering dielectronic-like recombination suggest that with the excep-

tion of the recombination line width, all of the Cas A carbon recombination line and  $\lambda 21$  cm H I absorption line data can be attributed to a region where the physical conditions are typical of the cold neutral medium of the ISM (Payne et al. 1994).

We also compared the [C I] emission with the H I distribution across Cas A (Schwarz et al. 1997). H I is observed in absorption across the entire Cas A disk and the morphology varies with the radial velocity with maximum optical depth being observed around  $-48.2$  km s $^{-1}$ . The peak absorption at this velocity arises in the south-east region which roughly coincides with the peaks seen in [C I] at similar velocity. H I absorption is also seen from the western half of Cas A with the peak shifted slightly towards the south. A similar peak is also observed in [C I] emission.

The [C I] distribution is thus partly similar to both H I and C270 $\alpha$  morphology. We compare the [C I] emission with the molecular component of the ISM traced by the CO emission in the next subsection.

### 3.4 Comparison of [C I] and molecular line emission toward Cas A

The left and middle panels of Fig. 6 show the distribution of  $^{13}\text{CO}$  1–0 and  $^{12}\text{CO}$  2–1 intensities (in contours) integrated between velocities of  $-50.3$  and  $-44.1$  km s $^{-1}$  (Liszt & Lucas 1999), superposed with the [C I] distribution (in grey). While the original resolution of the  $^{13}\text{CO}$  1–0 map is  $60''$ , the  $^{12}\text{CO}$  2–1 data has been smoothed to  $60''$ . In an earlier paper Wilson et al. (1993) observed the CO (and  $^{13}\text{CO}$ ) emission from the Perseus arm clouds in the direction of Cas A, with an angular resolution  $\sim 22''$ . The CO clouds identified by Wilson et al. (1993) are also marked by circles in Fig. 6. We note that the CO data from Liszt & Lucas (1999) do not show the clumped structure observed by Wilson et al. (1993) and we attribute it to the difference in resolution between the two datasets.

Figure 6 shows that the [C I] emission is detected from most of the CO emitting clouds and the [C I] peaks lie at the outer boundaries of the clumps. Substantial [C I] emission is detected with no corresponding CO emission from the diffuse PDRs to the north. The extreme right panel of Fig. 6 shows the integrated [C I] intensities overplotted with the CO clouds identified by Wilson et al. (1993). It clearly shows that although [C I] emission is detected from most of the clouds, the peaks of [C I] emission tend to lie at the boundaries of the CO clouds. We point out here that the CO clouds detected by Wilson et al. (1993) towards the western edge of the map belong to the  $-36$  km s $^{-1}$  Perseus arm feature, in contrast to the  $-47$  km s $^{-1}$  feature in [C I] emission being discussed in this paper. The relative position of the [C I] and CO emission peaks is consistent with the clumpy PDR scenario, in which PDRs form on the surface of the molecular clumps that are embedded in an interclump medium of lower density in which CO is dissociated to atomic carbon.

From the above comparisons it is clear that [C I] traces both CO and cold H I morphologies partially and is consistent with the PDR scenario when compared with the C $^+$  regions traced by the carbon recombination lines (e.g. C270 $\alpha$ ) and the molecular clouds traced by CO. We note here, that absorption studies of C RRLs necessarily imply that the emitting gas lies in front of the strong continuum emitting

SNR, no such restriction is however applicable to either the CO or the [C I] lines. Thus, beyond the similarities in the emission velocities of [C I] CO and the C270 $\alpha$  and the morphological similarity to a PDR-like structure, the present observations cannot conclusively rule out the possibility that the molecular (and neutral) and the ionized gas may not be occupying the same volume of gas.

## 4 NEUTRAL CARBON AND CO COLUMN DENSITIES

We have estimated the C $^0$  and CO column densities based on LTE approximation. For these calculations we have used the observed [C I] and  $^{13}\text{CO}$  1–0 line intensities and an excitation temperature,  $T_{\text{ex}}$ , of 20 K. Further we have assumed both [C I] and  $^{13}\text{CO}$  1–0 to be optically thin. The assumed  $T_{\text{ex}}$  of 20 K is justified because based on the  $^{12}\text{CO}$  and  $^{13}\text{CO}$  observations the kinetic temperatures of the molecular clumps in the Perseus arm along the direction of Cas A is  $\sim 20$  K (Wilson et al. 1993).

In the Perseus arm clouds with velocity  $\sim -47$  km s $^{-1}$  we estimate the column density of neutral carbon,  $N(\text{C})$ , to be between  $2 \times 10^{16}$  cm $^{-2}$  and  $1.3 \times 10^{17}$  cm $^{-2}$ . Near the [C I] peaks in the south-east and also to the west,  $N(\text{C})$  is larger than  $7 \times 10^{16}$  cm $^{-2}$ , while to the north and in the periphery of the [C I] emitting shell the column densities are close to  $3 \times 10^{16}$  cm $^{-2}$ .

Within the region mapped by us in [C I], the estimated  $^{13}\text{CO}$  column density (in a beam of  $1'$ ) varies between  $5 \times 10^{14}$  cm $^{-2}$  and  $9 \times 10^{15}$  cm $^{-2}$ . This corresponds to  $N(\text{CO})$  between  $3.0 \times 10^{16}$  cm $^{-2}$  and  $5 \times 10^{17}$  cm $^{-2}$ , assuming  $[^{12}\text{CO}/^{13}\text{CO}] = 60$ . The column density of  $^{13}\text{CO}$  derived from the  $1'$  dataset of Liszt & Lucas (1999) is slightly lower than the values obtained by Wilson et al. (1993), but matches reasonably well with the previous  $1.1' \ ^{13}\text{CO}$  1–0 observations by Troland et al. (1985).

Over the limited region in which the  $^{13}\text{CO}$  and [C I] emissions overlap, the C/CO abundance ratio varies between 0.08 and 1.8. At the positions of the CO clouds F and G the C/CO abundance ratio is  $\sim 0.2$ , a value typically found at the centre of dense cloud cores (Gerin et al. 1998; Oka et al. 2004). In the periphery of the CO clouds the value rises to 1.7 at positions where the [C I] emission peaks: this value is typical of the diffuse, translucent clouds (Ingalls et al. 1997; Bensch et al. 2003).

## 5 PDR INTERPRETATION OF THE OBSERVED [C I] EMISSION

The observed morphology of [C I] though not entirely correlated with the emission from the atomic or the molecular phases of the ISM, is consistent with the phenomenological understanding of PDR structure. [C I] is typically ubiquitous and towards the direction of Cas A, it appears to be arising from both the molecular clumps as well as the diffuse PDR. Most importantly, the [C I] emitting regions show no evidence for interaction with the SNR in Cas A. Here we explain the observed [C I] emission in terms of theoretical models for PDRs. We have used the plane-parallel models by Kaufman et al. (1999) for this purpose. The PDR model

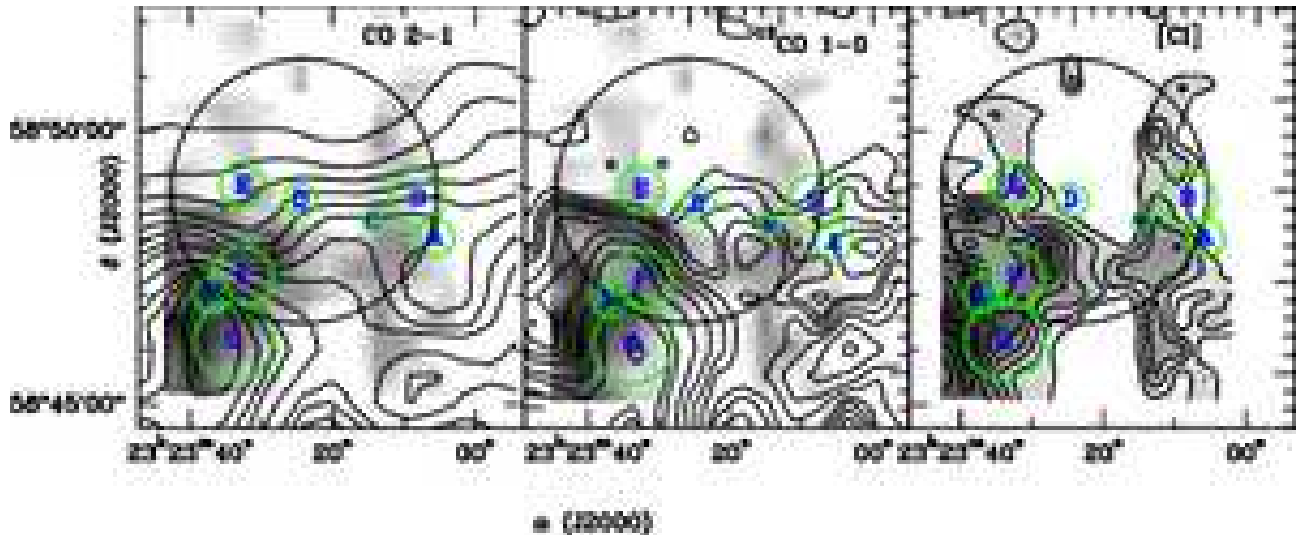


**Figure 6.** Integrated intensity distribution of [C I] (Grey) overlaid with integrated intensities of  $^{13}\text{CO}$  1-0 (left panel) and  $^{12}\text{CO}$  2-1 (middle panel) (Liszt & Lucas 1999). The  $^{13}\text{CO}$  1-0 data has a resolution of  $60''$ . The  $^{12}\text{CO}$  2-1 dataset has been smoothed to a resolution of  $60''$  for comparison. The large circle denotes the angular extent of Cas A. Extreme right panel shows both in grayscale and contours the integrated intensity of [C I]. The smaller circles in all panels show the position and sizes of CO clouds identified by Wilson et al. (1993).

used here takes into account a detailed chemical network, radiative transfer and thermal balance and considers a 1-dimensional slab of material exposed to a FUV radiation field in a face-on geometry. The plane-parallel PDR model calculates the intensity of various transitions of different chemical species as functions of two parameters, the local hydrogen density ( $n_{\text{PDR}}$ ) and the incident FUV radiation field. Kaufman et al. (1999) have created a database of PDR models, for local hydrogen densities  $n_{\text{PDR}}$ , between  $10$  &  $10^7 \text{ cm}^{-3}$  and FUV radiation field between  $0.3$  to  $3 \times 10^6 G_0$ , where  $G_0$  is the FUV flux measured in units of the “Habing field”, which is taken to be  $1.6 \times 10^{-3} \text{ erg cm}^{-2} \text{ s}^{-1} \text{ sr}^{-1}$  (Habing 1968).

In the absence of any nearby stars the far-ultraviolet (FUV) radiation field illuminating the [C I] emitting neutral atomic and/or molecular phase of the ISM will be of the order of  $1-5 G_0$ . For the following PDR analysis we assume the FUV flux to be  $\sim 1 G_0$ .

### 5.1 Hydrogen densities

We have used the observed  $\text{CI}/^{12}\text{CO}2-1$  intensity ratios to derive an independent estimate of the hydrogen volume densities in the [C I] emitting regions using the PDR models. For convenience from now on we split our discussion into two parts, the first deals with the south-eastern [C I] emitting regions which are largely concomitant with the CO emission and the second deals with the north-south stretching filamentary emission to the west of the map. The aim of this separation is also to look for possible differences between the two parts.

Figure 7 shows the distribution of the  $\text{CI}/^{12}\text{CO}2-1$  intensity ratios in regions where both intensities are more than three times the respective noise levels. Most of the pixels in both the south-eastern cloud and the western filament show intensity ratios between  $0.5$  and  $1.0$ . At the position of the

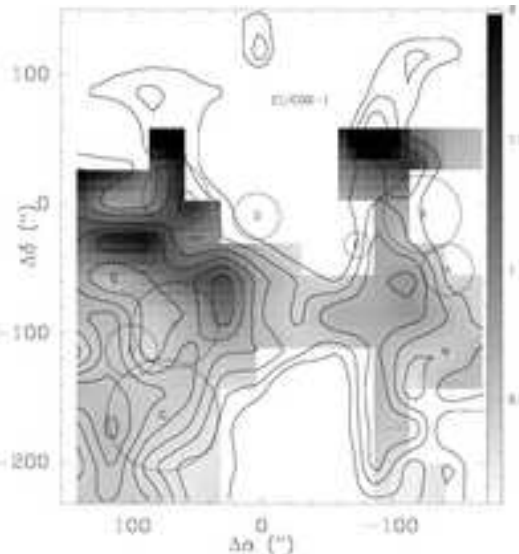


**Figure 7.** [C I]/ $^{12}\text{CO}2-1$  intensity ratio towards Cas A. Only positions with both [C I] and  $^{12}\text{CO}$  2-1 intensities larger than the  $3\sigma$  values for the respective maps are included. The contours of [C I] emission are overlaid for comparison. Also marked are the CO clouds identified by Wilson et al. (1993). The map is centred at the nominal centre being used throughout the paper, viz.,  $\alpha_{2000} = 23^{\text{h}}23^{\text{m}}24^{\text{s}}$ ;  $\delta_{2000} = +58^{\circ}48'9''$ .

[C I] emission peak to the south-east the ratio is  $1.3$  and towards the northern edge of the south-eastern cloud the ratio rises from  $1.8$  to  $4$ . In the western filament also the value rises to as high as  $4$  towards north. Clouds F, G and H show ratios of  $\sim 0.5$ , while cloud E has a value of  $\sim 1.3$ .

Figure 8 shows the variation of the  $\text{CI}/^{12}\text{CO}2-1$  intensity ratios as a function of the UV radiation field and the local hydrogen densities as estimated by the PDR models by Kaufman et al. (1999). For convenience we have drawn

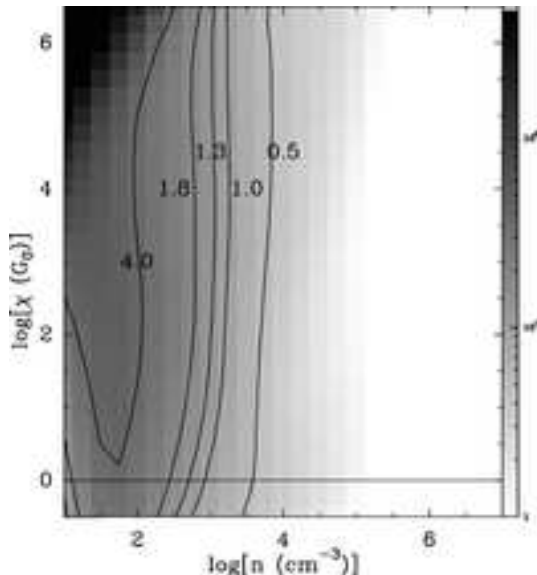


**Figure 8.** PDR model calculations of variation of  $\text{CI}/^{12}\text{CO}2-1$  intensity ratios as a function of hydrogen densities and incident UV radiation field (Kaufman et al. 1999). The contours (marked with their values) depict some of the typical ratios found toward Cas A. The horizontal line corresponds to the UV radiation field of  $1 G_0$ .

contours corresponding to some of the typical ratios found in the direction of Cas A. We note that according to the PDR models, the observed  $\text{CI}/^{12}\text{CO}2-1$  intensity ratio constrains the local hydrogen density almost independent of the UV radiation field assumed.  $\text{CI}/^{12}\text{CO}2-1$  intensity ratio of 4 or more corresponds to densities less than  $100 \text{ cm}^{-3}$ . The most commonly seen ratio of 0.5 suggests densities of the order of  $10^{3.5} \text{ cm}^{-3}$ . Thus the hydrogen density of the [C I] and CO emitting gas varies from 100 to  $3000 \text{ cm}^{-3}$ .

Since the [C I] emission only partially overlaps with the carbon RRL emission as well as the CO emission in a manner apparently consistent with the PDR scenario, it is interesting to compare the neutral hydrogen densities in the different regions. Based on latest models of carbon RRL emission, the atomic hydrogen densities are estimated to be around  $150 \text{ cm}^{-3}$ , for an electron temperature,  $T_e$ , of 75 K (Kantharia et al. 1998). CO observations suggest hydrogen volume densities of  $\sim 10^3 \text{ cm}^{-3}$  with localized higher densities (Wilson et al. 1993). We find that the southern parts of the mapped region [C I] emission arises primarily from regions in which hydrogen is mostly molecular with average densities of  $10^3 \text{ cm}^{-3}$ . To the north, the densities are lower and the [C I] emitting region has hydrogen primarily in the atomic phase. This is shown by the higher  $[\text{C I}]/^{12}\text{CO}2-1$  intensity ratios and the lower densities derived from the carbon RRL emission which peaks in this region and is known to arise in the atomic medium. The [C I] emission thus not only morphologically but also in terms of the continuity of density parameters acts as the transition phase between the atomic and the molecular phase of the neutral ISM.

## 5.2 Volume and Area Filling factors of the [C I] emission

In order to quantify our results better we have selected a few representative positions and derived densities at those positions for an UV field of  $\chi = 1 G_0$ . This analysis also aims to characterize the clumpy nature of the emitting regions along the lines of sight towards Cas A. The positions chosen correspond to the centres of the CO clouds E, F and G (Wilson et al. 1993) from which [C I] emission was clearly detected. In addition, we have chosen the primary [C I] peak in the entire mapped region, lying in the south-eastern molecular cloud and the secondary peak found to the north of the filamentary emission to the west. Finally we have chosen a representative position with average emission characteristics in the western filament.

Table 2 summarizes details of the selected positions and several parameters observed and derived from PDR models and obtained from literature.

As discussed in Sect. 5.1 the local hydrogen volume densities,  $n_{\text{PDR}}$ , at the selected positions are estimated from the observed  $\text{CI}/^{12}\text{CO}2-1$  intensity ratios using the PDR models (Col. 7, Table 2). We find  $n_{\text{PDR}}$  for the CO clouds F and G to be  $\sim 10^3 \text{ cm}^{-3}$ , while cloud E has a much lower density of only  $300 \text{ cm}^{-3}$ . These densities are in agreement with the values derived by Wilson et al. (1993) using much higher resolution ( $22''$ ) observations (Col. 12 Table 2). At the position of the two [C I] peaks to the south-east and in the western filament the densities are  $\sim 500 \text{ cm}^{-3}$ , while for most of the positions on the western filament the density is  $\sim 10^3 \text{ cm}^{-3}$ . This implies that the high [C I] intensities arise from the more diffuse interclump medium.

The  $\text{N}(\text{H}_2)$  per  $60''$  beam (Col. 5, Table 2) for the individual positions have been estimated as described in Sec. 4. For the clouds E & G the  $\text{N}(\text{H}_2)$  per beam ( $60''$ ) are lower by more than a factor of 3 than the  $\text{N}(\text{H}_2)$  measured per  $22''$  (Col. 11, Table 2) by Wilson et al. (1993), while for cloud F the two numbers agree. At those positions where the  $^{13}\text{CO} 1-0$  emission lies below the noise limits of the dataset, we have assumed the noise level to derive  $\text{N}(\text{H}_2) < 5.6 \times 10^{20} \text{ cm}^{-2}$ . Using the hydrogen column densities and assuming that the cloud extends the same distance along the line of sight as the linear size of the beam we have derived the beam-averaged volume densities ( $n_{\text{av}}$ ; Col. 6, Table 2). We note here that  $n(\text{H}_2)_{\text{wilson}}$  (Col. 12, Table 2) has also been derived from the  $\text{N}(\text{H}_2)_{\text{wilson}}$  in the same way.

The volume filling factors of the emitting clouds can be estimated as  $\phi_V = n_{\text{PDR}}/n_{\text{av}}$ . For most of the positions except for Cloud G and the average position in the western filament the volume filling factors are higher than 50% (Col. 10, Table 2). This is in contrast to the typical volume filling factors of 5% as found in the Galactic star forming regions (Kramer et al. 2004). The observed high volume filling factors thus indicate the rather diffuse nature of the [C I] emitting regions.

Comparison of the absolute [C I] intensities,  $I_{\text{CI,th}}$  (Column 7, Table 2), estimated by the PDR models which best reproduce the observed  $\text{CI}/^{12}\text{CO}2-1$  ratios, with the observed [C I] intensities ( $I_{\text{CI,obs}}$ ; Col. 4, Table 2) provides information about the area filling factors (Col. 9, Table 2) of the [C I] emitting clouds. The area filling factor is defined as:  $\phi_A = I_{\text{CI,obs}}/I_{\text{CI,th}}$ . At the selected positions in the direction

**Table 2.** Parameters observed and derived from PDR models at selected positions in the Perseus arm.  $n_{\text{PDR}}$  is local hydrogen volume density derived by comparing the observed  $\text{CI}^{12}\text{CO}_2-1$  intensity ratios with predictions of the PDR models.  $N(\text{H}_2)$  is the  $\text{H}_2$  column density per  $60''$  beam,  $\phi_A$  is the area filling factor of CI emission defined as  $I_{\text{CI,obs}}/I_{\text{CI,th}}$  and  $\phi_V$  is the volume filling factor defined as  $n_{\text{PDR}}/n_{\text{av}}$ . Quantities with the subscripts *wilson* are from Wilson et al. (1993).

(1)	(2)	(3)	(4)	(5)	(6)	(7)	(8)	(9)	(10)	(11)	(12)
Name	$\Delta\alpha$	$\Delta\delta$	$I_{\text{CI,obs}}$	$N(\text{H}_2)$	$n_{\text{av}}$	$n_{\text{PDR}}$	$I_{\text{CI,th}}$	$\phi_A$	$\phi_V$	$N(\text{H}_2)_{\text{wilson}}$	$n(\text{H}_2)_{\text{wilson}}$
	"	"	$\text{K km s}^{-1}$	$10^{20} \text{ cm}^{-2}$	$\text{cm}^{-3}$	$\text{cm}^{-3}$	$\text{K km s}^{-1}$			$10^{20} \text{ cm}^{-2}$	$\text{cm}^{-3}$
Cloud E	58.	0.	5.0	5.6	180	300	10.9	0.5	0.6	20	<800
Cloud F	58.	-87.	5.3	39	1200	2000	14.1	0.4	0.6	40	1000
Cloud G	87.	-174.	6.7	52	1600	5000	13.0	0.5	0.3	90	2000
CI Peak West	-87.	29.	2.9	5.6	180	400	10.9	0.3	0.5		
CI Peak SE	29.	-87.	8.1	18	560	630	12.6	0.6	0.9		
CI West Avg	-87.	-58.	4.8	11	340	1778	14.1	0.3	0.2		

towards Cas A the [C I] area filling factor is on an average equal to 0.5.

## 6 SUMMARY

We have used the [C I] emission at 492 GHz to probe the PDRs seen in the direction of the supernova remnant Cas A. We detect [C I] emission at velocities around  $-47$  and at  $-39 \text{ km s}^{-1}$  from the Perseus arm clouds, and at  $-1 \text{ km s}^{-1}$  from the local Orion arm cloud. The [C I] emission does not show any strong morphological correlation with the continuum emission from Cas A. Further, we do not detect any obvious broadening or strengthening of spectral lines closer to the continuum peak. Both of these conclusively rule out that the [C I] emitting gas is interacting with the SNR in Cas A.

We detect [C I] emission from both the diffuse CNM (as traced by the C RRLs) and the denser molecular cloud. Morphological comparison of the [C I] emission with the carbon RRL ( $\text{C}270\alpha$ ), H I optical depth and CO distribution appear to be consistent with a PDR scenario in which the dominant carbon-bearing species changes from  $\text{C}^+$  in the diffuse region through  $\text{C}^0$  to CO in the more dense molecular clumps. We note with caution that despite the morphological and kinematic evidences the present observations cannot rule out the possibility that the [C I] and C RRL emitting regions may not completely occupy the same volume of space.

We estimate the  $\text{C}^0$  column density,  $N(\text{C})$ , to be between  $2 \times 10^{16}$  and  $1.3 \times 10^{17} \text{ cm}^{-2}$ . At the position of the previously identified CO clouds we estimate the C/CO abundance ratio to be around 0.2, similar to the typical value found in dense cloud cores. Most of the [C I] emitting region however shows C/CO abundance ratios  $> 1$ , typical of diffuse, translucent clouds.

We have derived hydrogen volume densities of the [C I] emitting regions from the  $[\text{C I}]/^{12}\text{CO}_2-1$  intensity ratios using PDR models. We find that the local hydrogen densities vary from  $\sim 10^2 \text{ cm}^{-3}$  near the [C I] peaks to  $10^{3.5} \text{ cm}^{-3}$  around CO peaks. This also shows a continuity in the density structure in the region between the the diffuse C II region and the denser molecular clouds. We estimate the area filling factor of the [C I] emitting regions to be  $\sim 0.3$ , while the volume filling factor is on an average  $> 30\%$ . This fur-

ther suggests that most of the [C I] emission stems from the diffuse PDR also traced by the carbon recombination lines.

## ACKNOWLEDGMENTS

We thank the referee, Jay Lockman, for comments which improved the clarity and presentation of the paper. We thank H. Liszt for allowing us to use the CO datasets. This material is based upon work supported by the Deutsche Forschungs Gemeinschaft (DFG) via grant SFB494 and the National Science Foundation under Grant No. AST-0228974. This research has made use of NASA's Astrophysics Data System.

## REFERENCES

- Anantharamaiah, K. R., Erickson, W. C., Payne, H. E., Kantharia, N. G., 1994, *ApJ*, 430, 682.  
 Andersson, B.-G., & Wannier, P. G. 1993, *ApJ*, 402, 585  
 Bensch, F., Leuenhagen, U., Stutzki, J., & Schieder, R. 2003, *ApJ*, 591, 1013  
 Blake, D. H., Crutcher, R. M., Watson, W. D., 1980, *Nature*, 287, 707  
 Dickey, J. M., & Lockman, F. J. 1990, *ARA&A*, 28, 215  
 Ershov, A. A., Lekht, E. E., Smirnov, G. T., Sorochenko, R. L. 1987, *Sov. Astron. Lett.*, 13, 8  
 Gerin, M., Phillips, T. G., Keene, J., Betz, A. L., & Boreiko, R. T. 1998, *ApJ*, 500, 329  
 Habing, H. J. 1968, *Bull. Astr. Inst. Netherlands*, 19, 421  
 Hollenbach, D. J., Tielens, A. G. G. M. 1999, *Rev of Mod Phys.*, 71, 173.  
 Howe, J. E., Jaffe, D. T., Genzel, R., & Stacey, G. J. 1991, *ApJ*, 373, 158  
 Ingalls, J. G., Chamberlin, R. A., Bania, T. M., et al., 1997, *ApJ*, 479, 296  
 Kantharia, N. G., Anantharamaiah, K. R., Payne, H. E., 1998, *ApJ*, 506, 758  
 Kaufman, M. J., Wolfire, M. G., Hollenbach, D. J., Luhman, M. L., 1999, *ApJ*, 527, 795  
 Kassim, N. E., Perley, R. A., Dwarakanath, K. S., & Erickson, W. C. 1995, *ApJ*, 455, L59  
 Konvalenko, A. A., Sodin, L. G., 1980, *Nature*, 283, 360  
 Kramer, C., Jakob, H., Mookerjea, B., et al., 2004, *A&A*, 424, 887



- Kulkarni, S. R., & Heiles, C. 1987, *ASSL Vol. 134: Interstellar Processes*, 87
- Liszt, H., & Lucas, R. 1999, *A&A*, 347, 258
- McKee, C. F., Hollenbach, D., & Wolfire, M. G. 2004, *The Dense Interstellar Medium in Galaxies*, 395
- Mookerjee, B., Ghosh, S. K., Kaneda, et al., 2003, *A&A*, 404, 569
- Moriarty-Schieven, G. H., Andersson, B.-G., & Wannier, P. G. 1997, *ApJ*, 475, 642
- Oka, T., Iwata, M., Maezawa, H., et al., 2004, *ApJ*, 602, 80
- Pankonin, V., Barsuhn, J., Thomasson, P., 1977, *A&A*, 54, 335
- Payne, H. E., Anantharamaiah, K. R., Erickson, W. C., 1989, *ApJ*, 341, 890
- Payne, H. E., Anantharamaiah, K. R., Erickson, W. C., 1994, *ApJ*, 430, 690
- Schwarz, U. J., Goss, W. M., & Kalberla, P. M. W. 1997, *A&AS*, 123, 43
- Schröder, K., Staemmler, V., Smith, M. D., Flower, D. R., & Jaquet, R. 1991, *Journal of Physics B Atomic Molecular Physics*, 24, 2487
- Troland, T. H., Crutcher, R. M., & Heiles, C. 1985, *ApJ*, 298, 808
- Wilson, T. L., Mauersberger, R., Muders, D., Przewodnik, A., & Olano, C. A. 1993, *A&A*, 280, 221
- Wolfire, M. G., McKee, C. F., Hollenbach, D., & Tielens, A. G. G. M. 2003, *ApJ*, 587, 278
- Wyrowski, F., Walmsley, C. M., Goss, W. M., & Tielens, A. G. G. M. 2000, *ApJ*, 543, 245